Temperature-Swing Synthesis of Large-Size Single-Crystal $LiNi_{0.6}Mn_{0.2}Co_{0.2}O_2$ Cathode Materials

Guannan Qian,[1,2,=] Zhiyuan Li,[1,=] Dechao Meng,[1] Jia-bing Liu,[3] Yu-Shi He,[1] Qunli Rao,[4] Yijin Liu,[2] Zi-Feng Ma,[1,z] and Linsen Li[1,z]

[1] *Department of Chemical Engineering, Shanghai Electrochemical Energy Device Research Center (SEED), Shanghai Jiao Tong University, Shanghai 200240, People's Republic of China*
[2] *Stanford Synchrotron Radiation Lightsource, SLAC National Accelerator Laboratory, Menlo Park, California 94025, United States of America*
[3] *Lava Energy Technology Corporation, Suzhou, Jiangsu, 215129, People's Republic of China*
[4] *Instrumental Analysis Center, Shanghai Jiao Tong University, Shanghai 200240, People's Republic of China*

Single-crystal lithium-nickel-manganese-cobalt-oxide (SC-NMC) has recently emerged as a promising battery cathode material due to its outstanding cycle performance and mechanical stability over the tradional polycrystalline NMC. It is favorable to further increase the grain size of SC-NMC particles to achieve a higher volumetric energy density and minimize surface-related degradations. However, the preparation of large-size yet high performance SC-NMC particles faces a challenge in choosing a suitable temperature for sintering. High temperature promotes grain growth but induces cation mixing that negatively impacts the electrochemical performance. Here we report a temperature-swing sintering (TSS) strategy with two isothermal stages that fulfils the needs for grain growth and structural ordering sequentially. A high-temperature sintering is first used for a short period of time to increase grain size and then the reaction temperature is lowered and kept constant for a longer period of time to improve structural ordering and complete the lithiation process. SC-$LiNi_{0.6}Mn_{0.2}Co_{0.2}O_2$ materials prepared via TSS exhibit large grain size ($\sim$4 μm), a low degree of cation mixing ($\sim$0.9%), and outperform the control samples prepared by the conventional sintering method. This work highlights the importance of understanding the process-structure-property relationships and may guide the synthesis of other SC Ni-rich cathode materials.

The depletion of fossil fuel and the increasing carbon footprint have motivated tremendous efforts in developing electric transportation globally. Lithium-ion batteries (LIBs) have demonstrated great potential and are the dominant power sources for electric vehicles (EVs). Its success benefits from the high energy and power densities, environmental friendliness, and (increasingly) affordable cost. For EV batteries, layered transition metal oxide (LTMO) is a technologically important cathode material, which is continuously being studied and improved to meet the growing demand towards high energy density and safety.[1,2] The Ni-rich layered oxides [$LiNi_xCo_yM_{1-x-y}O_2$ ($x \geqslant 0.6$, M = Mn or Al), NMC or NCA] possess a specific capacity of over 180 mAh g^{-1} (at 4.3 V vs Li^+/Li) and a relatively high discharge plateau ($\sim$3.7 V), enabling more than 50% energy density compared with the olivine-structured $LiFePO_4$ (LFP).[3,4] However, the cycle performance of typical NMCs is inferior to LFP (approximately 1500 − 2500 cycles vs at least 5000−6000 cycles). Ni-rich NMCs are known to suffer from surface phase transitions,[5,6] micro-cracks along grain boundaries,[7–9] and undesired interfacial side reactions with electrolytes.[10,11] To address these issues, many different approaches have been developed, including doping foreign elements into the lattice,[12–15] surface coating,[16–18] tuning the compositional gradients,[19,20] regulating the crystal orientation of the primary particles,[21–23] and making single-crystal-like particles.[24,25] Among them, the use of single-crystal NMC (SC-NMC) has emerged as an effective strategy to improve the electrochemical stability for LIBs and quickly attracted a lot of attention recently.[24] Polycrystalline NMCs are prepared in the form of spherical-shaped secondary particles made of numerous nanoscale primary grains and thus contain a large number of grain boundaries, which are the chemical and mechanical weak points vulnerable to cracks due to the heterogeneous strain upon cycling, causing impedance growth and performance decay.[26] The SC strategy eliminates internal grain boundaries in NMC particles and have led to significantly improved structural and electrochemical stability.[27,28]

SC-NMC materials can be made either by solid-state or molten-salt-assisted (MSA) synthesis.[25,26,29–31] In order to promote particle sintering and increase grain size, the solid-state approach normally uses a reaction temperature higher than the optimal one from the point view of electrochemical performance. For example, SC-$LiNi_{0.6}Mn_{0.2}Co_{0.2}O_2$ (NMC622) materials were prepared at 940 °C instead of 900 °C,[25] which was reported to produce high-performance samples.[32] It was previously reported that high temperature would lead to structural disorder and formation of rock-salt impurity phases, which negatively impacted the electrochemical performance.[33] In addition, it is quite difficult to control the particle size or morphology in the solid-state synthesis. The SC-NMC622 materials prepared by the solid-state approach became "brick"-like chunks after sintering and needed to be pulverized, ground, and sieved to achieve an acceptable level of particle size distribution.[25] By contrast, MSA synthesis uses molten-salts as medium for ion diffusion and reaction, which promotes the formation of SC-like particles with high crystallinity and a uniform grain size.[34,35] MSA synthesis has been used to make many functional materials, including ceramics,[36] metal carbides or nitrides,[37] and metal chalcogenides.[38] For the synthesis of SC-NMCs, Kim first applied this method to synthesize SC-NMC811 in a flux of KCl or NaCl. The SC-NMC811 particles shows well-formed facet planes, a morphology quite different from the polycrystalline NMCs.[29] Kimijima et al. systematically investigated how different reaction conditions, such as salts, precursor/salt molar ratios, reaction temperature, and reaction time, would impact the shape of SC-NMC333 during synthesis.[39,40] Zhu et al. synthesized SC-NMCs with different Ni content via the MSA method and studied the impact of surface facets on cycle stability during high-voltage operation.[41] Recently, we have reported the synthesis of SC-NMC622 in molten LiOH-Li_2SO_4 at 900 °C. The SC-NMC622 particles were $\sim$1−2 μm in size and showed excellent cycle performance and rate capability.[26] To achieve higher packing density and volumetric energy density, it is favorable to further

[=] These authors contributed equally to this work.
[z] E-mail: zfma@sjtu.edu.cn; linsenli@sjtu.edu.cn

increase the grain size of the SC NMC particles. However, it is a non-trivial task in designing the synthesis as it faces a dilemma in choosing a suitable reaction temperature. High temperature favors formation of large-size grains but can introduce undesired cation mixing in the lattice structure that hurts the electrochemical performance.

To tackle the aforementioned challenge in synthesis, here we propose a temperature-swing sintering (TSS) strategy with two isothermal stages that fulfils the needs for grain growth and structural ordering sequentially. In our TSS approach, a high-temperature sintering is first used for a short period of time to promote grain growth and then the reaction temperature is lowered and kept constant for a longer period of time to improve structural ordering and complete the lithiation process. This TSS method is distinct from the conventional ones used for NMC synthesis, which normally involve only one isothermal sintering step. In this work, we demonstrate the TSS method using SC-NMC622 as a model material. The as-prepared SC-NMC622 material shows large particle size of ~4 μm yet maintain a low degree of cation mixing (~0.9%), which leads to improved electrochemical performance over the control samples prepared via conventional sintering methods. This work highlights the importance of understanding the process-structure-property relationships and may guide the synthesis of other SC Ni-rich cathode materials.

Experimental

Materials.—The $Ni_{0.6}Mn_{0.2}Co_{0.2}(OH)_2$ hydroxide precursor was acquired from Reshine New Material Co. Ltd ($D_{50} \approx 3.5$ μm). The N-methyl-2-pyrrolidinone (NMP), LiOH, and Li_2SO_4 were purchased from Adamas. Polyvinylidene Fluoride (PVDF), Super-P (carbon black), battery-grade electrolytes, and lithium foils were purchased from Shanghai Songjing New-Energy Technology Company.

Synthesis of single-crystal $LiNi_{0.6}Mn_{0.2}Co_{0.2}O_2$ materials.— *Synthesis of SC-1000TSS.*—0.02 mol of $Ni_{0.6}Mn_{0.2}Co_{0.2}(OH)_2$ was manually mixed with 0.03 mol of LiOH and 0.005 mol of Li_2SO_4 by grinding. The mixture was loaded into an alumina crucible with a loosely covered lid and heated to 1000 °C at a ramping rate of 10 °C min^{-1} in air and held at 1000 °C for 3 h. Then, the temperature was lowered to 900 °C at a rate of 2 °C min^{-1} and kept constant for 10 h before cooling. The cooling rate was at 2 °C min^{-1} from 900 °C to 300 °C. After that, the material was cooled down naturally. Powders were recovered from the crucible, manually ground, and washed using deionized water to remove the excess Li-salts. The obtained powders were dried at 80 °C in air and then thermally treated at 500 °C for 5 h in air. The as-made powders was ground, passed through a 400-mesh sieve, and finally stored in a humidity-controlled box before further testing.

Synthesis of SC-900 and SC-1000.—The preparation methods of SC-900 and SC-1000 samples were the same as the one for SC-1000 TSS except the sintering temperature and reaction time. These two samples were sintered at 900 °C and 1000 ° respectively for 15 h in air. Same heating and cooling rates were used.

Characterizations.—ICP-AES was tested on an iCAP™ 7600-OES Analyzer (Thermo Fisher). SEM was performed on a scanning electron microscope (MIRA3 TESCAN). The imaging mode is second electron with 5 kV of the acceleration voltage. XRD was carried out using an X-ray diffractometer (Bruker D8, Cu Kα radiation) and scanned from 15 to 120 ° a step size of 0.01 °. XRD data was analyzed by the Rietveld refinement program of GSAS/EXPGUI software.[42] The tap density was measured using a tap density analyzer (ZS-201, Liaoling Instrument). In order to measure the compact density, we pressed ~1 g of powders into pellets using a custom-built mold (13 mm in diameter) under a pressure of ~5 ton cm^{-2} and measured the thickness (h) of the pellets to calculate their volume (V). Then, the compact density is determined by the following equation $\left(\rho = \frac{m}{V}\right)$.

Electrochemical measurements.—To make the composite cathode, the SC NMC material was homogeneously mixed with Super-P carbon black and PVDF with a weight ratio of 90:5:5 in NMP by a Thinky Mixer (ARE-310). The slurries were coated onto aluminum foils using a film applicator before being dried in an air-convection oven at 80 °C for 1 h and kept under vacuum at 120 °C for 10 h. The electrodes were pressed and cut into discs with an

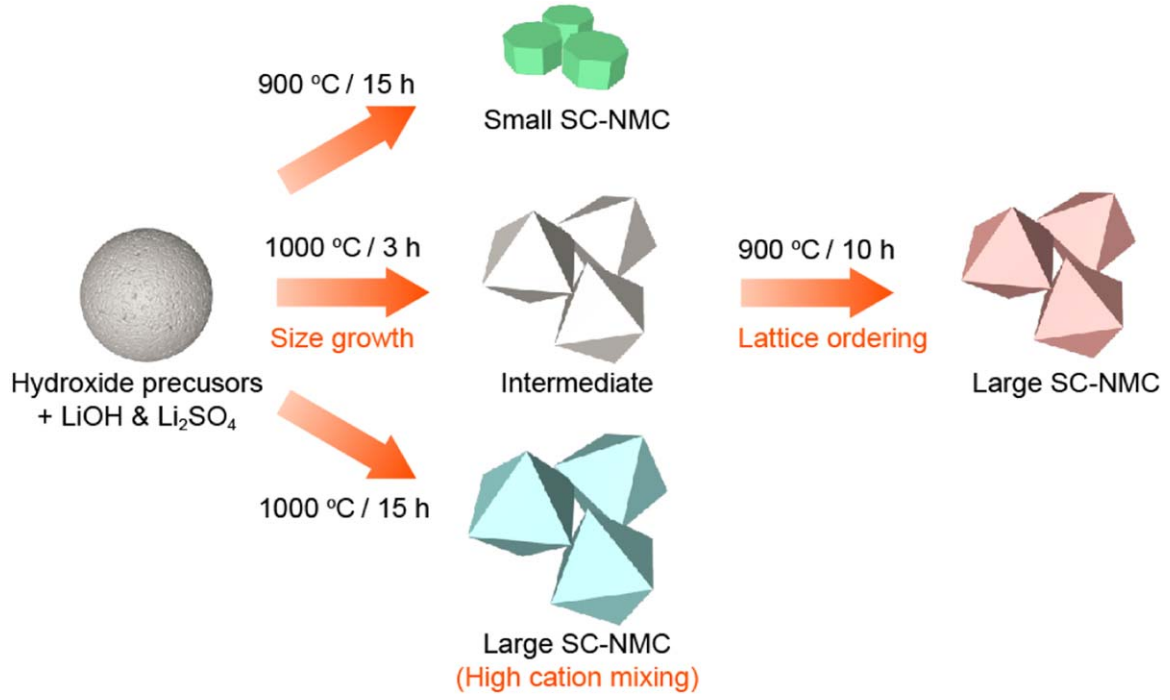

Figure 1. Schematic illustration of the temperature-swing sintering (TSS) method and the conventional method that only involves one iso-thermal annealing step.

active loading of 3−4 mg cm^{-2}. Half cells were assembled using Li foil (0.45 mm in thickness) as the anode, a polyethylene separator, and 1.2 M $LiPF_6$ dissolved in EC: EMC (3:7 by weight) + 2 wt% VC as the electrolyte in an argon-filled glove-box (Mikrona, O_2 and H_2O < 0.1 ppm). Electrochemical tests were carried out using battery cyclers (Shenzhen Neware, BTS4000–5 V, 10/1.0 mA version). The 2032-coin cells were cycled inside temperature chambers set at 30 °C. The half-cells were cycled at 0.1 C for three cycles before cycling at 1 C (1 C = 180 mA g^{-1})

Results and Discussion

The TSS method is schematically shown in Fig. 1 in comparison with the conventional methods. In TSS, the metal hydroxide precursors, lithium hydroxide (LiOH), and lithium sulfate (Li_2SO_4, serving as the molten salt) were mixed and first heated at 1000 °C for 3 h to promote grain growth (see Experimental section for details). Then the reaction temperature was lowered to 900 °C and held for ∼10 h before cooling. 900 °C is considered as an optimal temperature for synthesizing high-performance NMC622 according to our previous work.[26] For the sake of comparison, we also prepared two control samples: one at 900 °C for 15 h and the other at 1000 °C for 15 h. The samples were labeled as SC-1000TSS, SC-900, and SC-1000, respectively.

We checked the particle size and morphology of the three samples using scanning electron microscopy (SEM, Fig. 2). All three samples showed relatively homogeneous particle size and little particle agglomeration. The shape of SC-900 particles is plate-like with large-area (003) surfaces and the particle size is in a range of 1 −2 μm, which is consistent with our previous work.[26] The TSS method produced polyhedral particles (SC-1000TSS) with a larger particle size of 3−4 μm compared with SC-900, which confirmed the viability of the TSS method in increasing grain size. The change in particle shape from plate to polyhedron is most likely an effect of temperature, which was observed in the NMC and $LiCoO_2$ material systems previously.[41,43,44] The particle size could be further increased when the materials were sintered at 1000 °C for 15 h (SC-1000). The tap density and compact density of the three samples were measured and the results are summarized in Table I. These results reveal that the particle size and morphology of the SC-NMC622 are dependent on reaction temperature and time, which may be tuned to optimize its physical and electrochemical properties.

It has been recognized that the stoichiometry of the NMC materials has a direct impact on their electrochemical performance.[26] We measured the element composition of the three samples using induced coupled plasma-optical emission spectroscopy (ICP-OES). The results are summarized in Table II. The molar ratios among Ni, Co, and Mn were all close to 0.6:0.2:0.2 for the three samples. The Li/(Ni + Mn + Co) molar ratios were close to 1:1. The three samples showed the expected elemental composition despite being slightly over-lithiated. We note that a large excess of Li in NMC [$Li_{1+x}NMC_{(1-x)}O_2$] should be avoided, because it would induce more Ni^{3+} and reduce the accessible redox capacity.

To investigate the impact of different sintering methods on structural ordering, XRD measurements were carried out. All three samples exhibited a highly-ordered hexagonal α-$NaFeO_2$ type of structure with $R\bar{3}m$ symmetry without any detectable impurity phase (Fig. 3). The XRD patterns were further analyzed by Rietveld refinements. In the refinement process, the sum of Li and Ni atoms in Li slab was constrained to 1 (Li1+Ni2 = 1). As shown in Figs. 3a –3c, the lattice parameters have a strong correlation with the sintering temperature. The lattice parameter ***a*** and ***c*** for SC NMC increased with the holding time at 1000 °C. We calculated the ratio of Ni atoms occupying the Li sites (Ni_{Li}, see crystal structure in Fig. 3d) based on the refinement results, which has been used to evaluate the degree of cation mixing and structural ordering of NMC.[25] The Ni_{Li} values for SC-900, SC-1000TSS, and SC-1000 were 1.0%, 0.9%, and 3.0%. It is clear that an isothermal sintering at 1000 °C for 15 h (SC-1000) induce more cation mixing in NMC and therefore should be the least favorable for synthesis. SC-1000TSS (1000 °C for 3 h + 900 °C for 11 h), however, exhibited a Ni_{Li} of 0.9%, comparable to that of SC-900 (1.0%). We also probed the surface of the single-crystal NMC particles. Soft X-ray absorption spectra from the SC-1000 and SC-1000TSS samples were recorded using the total electron yield detector (TEY mode). The probing depth is ∼5 nm in the TEY mode. The sample heated at 1000 °C for 15 h (SC-1000) indeed had more Ni^{2+} (i.e. more NiO-like rock-salt phase at the surface) at the surface than SC-1000TSS (1000 °C for 3 h + 900 °C for 10 h), as indicated by the intensity ratio between the L_3-high and L_3-low peaks (Fig. S1 (available online at stacks.iop.org/JES/168/010534/mmedia)).

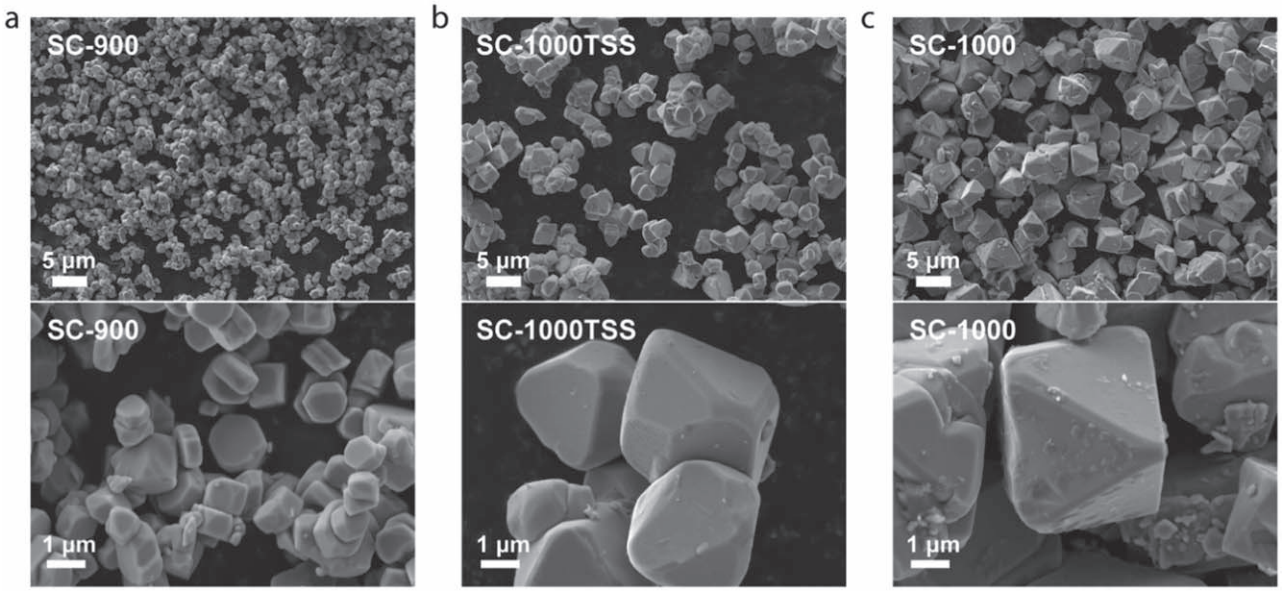

Figure 2. SEM images of the SC-NMC622 samples. (a) SC-NMC622 prepared at 900 °C for 15 h; (b) SC-NMC622 prepared by the temperature-swing sintering (TSS) method. The sample was first sintered at 1000 °C for 3 h and then cooled down to 900 °C and held at 900 °C for 10 h before cooling; (c) SC-NMC622 prepared at 1000 °C for 15 h.

Table I. Tap density and compact density of the SC-NMC622 samples.

Sample	Tap Density (g cm^{-3})	Compact Density (g cm^{-3}) at 5 ton cm^{-2}
SC-900	1.72	3.06
SC-1000TSS	1.92	3.31
SC-1000	2.00	3.46

Table II. Elemental composition of the three samples shown in molar ratio.

Sample	Li	Ni	Co	Mn
SC-900	1.03	0.60	0.20	0.20
SC-1000TSS	1.04	0.60	0.20	0.20
SC-1000	1.04	0.59	0.20	0.21

are affected by several other experimental parameters, such as peak broadening, peak asymmetry, and preferred orientation. The SC NMC samples clearly show preferred orientation. Therefore, this method is not reliable and Rietveld refienment is a better choice.

Figure 4 shows the magnified views of selected regions of the XRD patterns for the three samples, in which the hollow circles and line represent the experimental data and calculated results, respectively. The full width at half maximum (FWHM) of (003) plane is related to the crystallinity of the materials. SC-1000TSS has the smallest FWHM of 0.0888, which is indicative of good crystallinity.

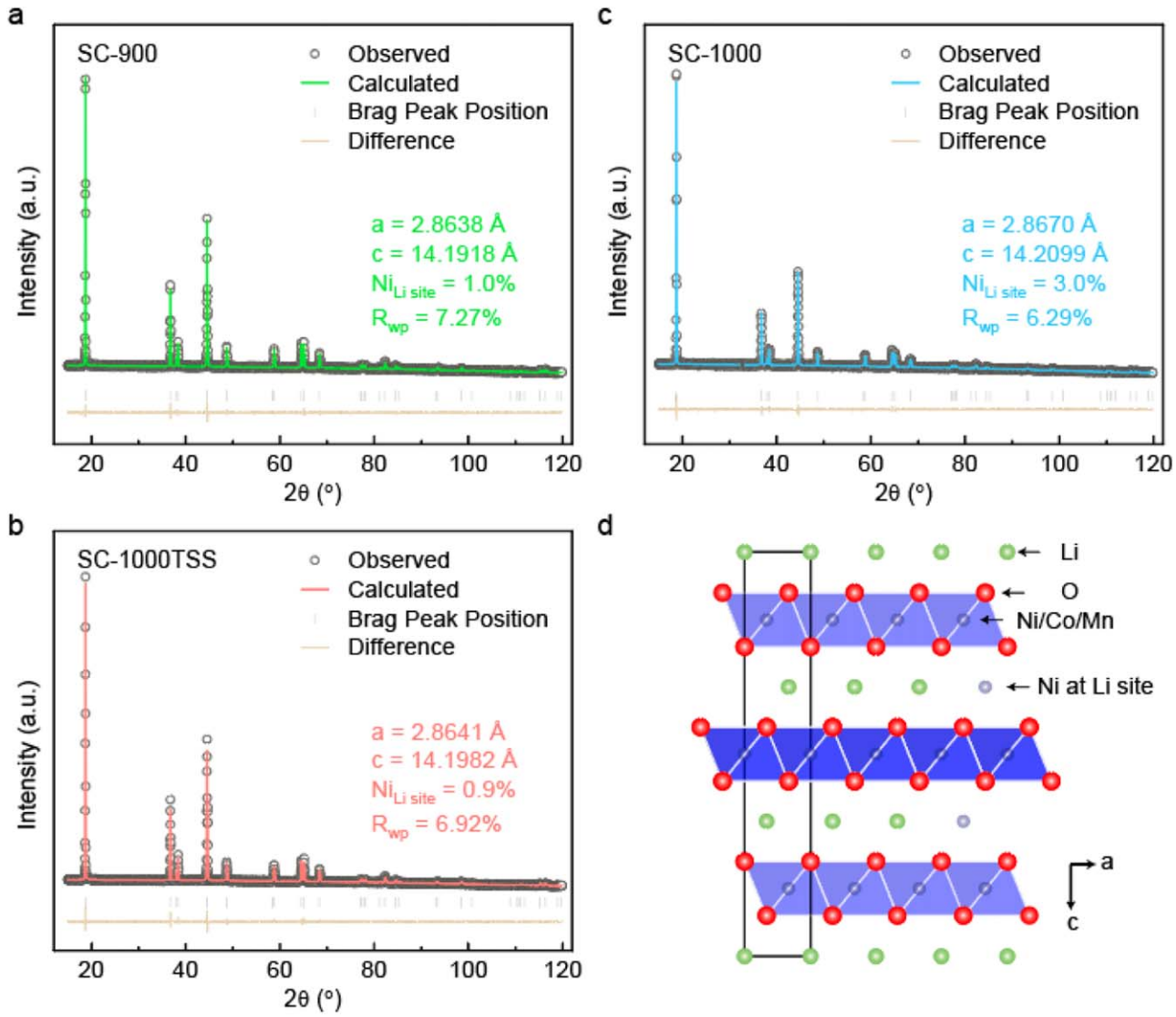

Figure 3. XRD patterns and Rietveld refinement results. (a) SC-900; (b) SC-1000TSS; (c) SC-1000; (d) Crystal structure of NMC viewed along [010] direction.

We also note that the (003)/(104) peak intensity ratio has been widely used as an indicator for the ordering of the layered structure. However, this calcuation method only considers the structural factors. Diffraction peak intensities at different scattering angles The $K_{\alpha1}$ and $K_{\alpha2}$ splitting of the (104), (108), and (110) peaks is also a fingerprint for good crystallinity. The peak splitting is clearly seen in SC-900 and SC-1000TSS but not in SC-1000. These results from XRD measurements and refinements confirmed that the TSS method

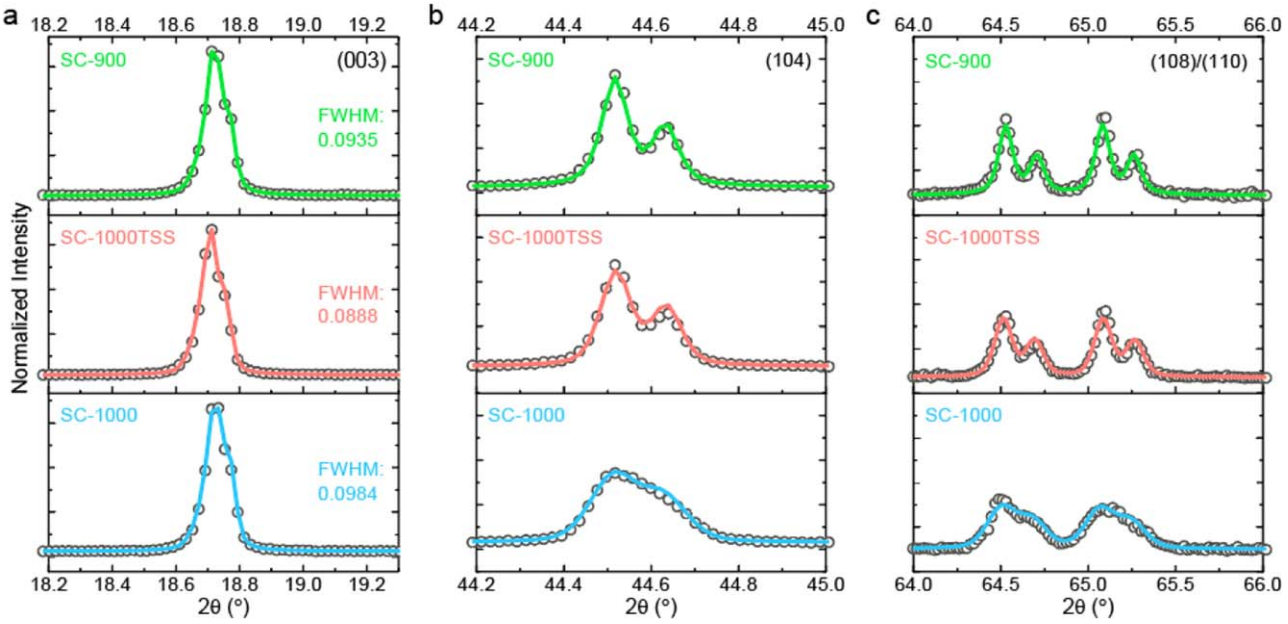

Figure 4. Magnified views of selected regions of the XRD patterns for the SC-900, SC-1000TSS, and SC-1000 samples. Panel (a) shows the (003) peaks; Panel (b) shows the (104) peaks; Panel (c) shows the (108) and (110) peaks. Black circles are experimental data. Colored lines are fitting results from Rietveld refinements.

could produce SC-NMC622 with low cation mixing, so that the grain growth and structural ordering processes were effectively decoupled.

To investigate the relationships between sintering methods, structure, and electrochemical performance, galvanostatic charge-discharge tests were performed in the voltage range of 4.3−2.8 V in half cells. Figure 5a shows the first-cycle charge and discharge voltage curves of the SC-900, SC-1000TSS, and SC-1000 samples, which delivered specific discharge capacities of 180, 183, and 174 mAh g^{-1} respectively at a current density of 0.1 C (18 mA g^{-1}). The first-cycle coulombic efficiencies (CE) of the three samples were 89.5%, 90.3%, and 88.0%. SC-1000TSS showed the highest capacity and CE among the three samples. It also exhibited the smallest polarization, which could be seen in the voltage curve (Fig. 5a) and the dQ/dV plots (Fig. 5b). Upon cycling at a current density of 1 C, all three samples showed good cycle performance (Fig. 5c). In particular, the SC-1000TSS sample delivered a discharge capacity of 168 mAh g^{-1} at 1 C and retained 96% of its capacity after 80 cycles, which was better than the two samples synthesized by the conventional sintering method (87% for SC-900 and 91% for SC-1000) and among the best reported for SC-NMC622 materials (see the comparison in Table SI). The electrochemical measurement results are consistent with those from XRD and refinement analysis. SC-NMC622 particles with large size and a low degree of Ni_{Li} prepared by the TSS method stand out for stable cycle performance and a high capacity. We also tested the high-voltage cycling performance of the SC-1000TSS sample and observed ∼20% of capacity loss after 80 cycles (4.5–2.8 V cycling at 1 C, see Fig. S2). Clearly, coating and/or doping strategies are necessary for high-voltage cycling. Recently, we have shown that surface Zr^{4+} doping combined with ZrO_2 coating significantly improved the high-voltage cycle performance of the SC-NMC622 cathode (98.5% retention after 150 cycles at 1 C).[45] With increasing grain size, rate capability may become a concern for the SC-NMC cathode.[46] The SC-1000TSS cathode was charged and discharged several different C-rates (0.1, 0.5, 1, 3, 5, and 10 C) and showed reasonable rate performance (Fig. S3). It could still deliver a specific capacity of ∼160 mAh g^{-1} during 3 C/3 C cycling (∼87% of the capacity at 0.1 C/0.1 C). The results are consistent with those reported by H. Li et al. in Ref. 25.

Conclusions

We have proposed and developed a TSS strategy to decouple grain growth and structural ordering processes and produced large-

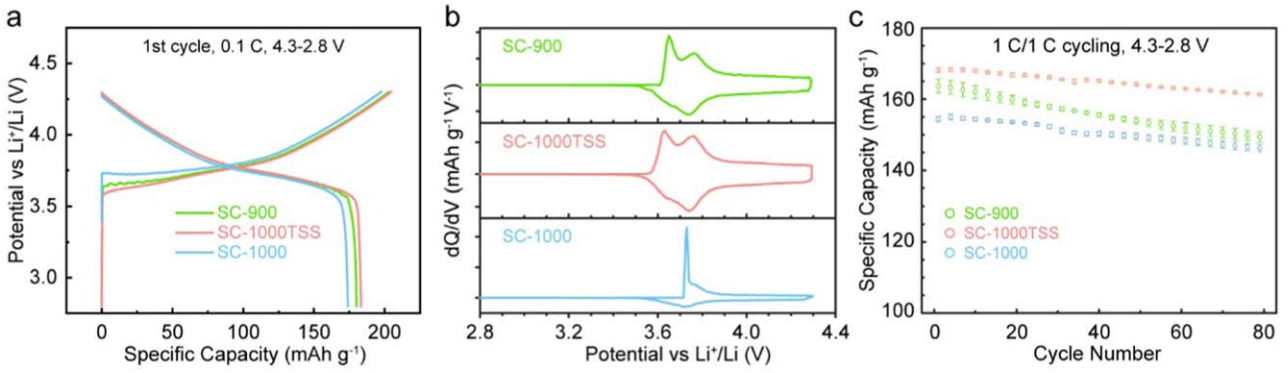

Figure 5. (a) 1st-cycle charging/discharging curves of SC-900, SC-1000TSS, and SC-1000 at 0.1 C between 4.3 and 2.8 V; (b) The differential capacity as a function of voltage (dQ/dV plots) for the three samples; (c) Cycle performance of the three samples at 1 C. Three cells were tested in each case. (1 C = 180 mA g^{-1}).

size SC-NMC622 particles with a low degree of cation mixing. XRD measurements and Rietveld refinement analysis confirmed that a short period of high-temperature sintering followed by a longer period of sintering at lower temperature did not have a negative impact on structural ordering or lead to formation of impurity phases. As a result, the SC-NMC622 prepared via TSS exhibited high specific capacity, high CE, low polarization, and good cycle performance, outperforming the control samples prepared by the conventional method that only involves sintering at one constant temperature. Our results highlight the importance of mechanistic studies into the preparation process of SC-NMCs, which is slightly different from that of the polycrystalline NMC. A good control over both grain size (equal to particle size in SC-NMC) and structural ordering is needed in synthesizing high-performance SC-NMCs, whereas the particle size of the polycrystalline NMCs is largely decided by the hydroxide precursors and does not change significantly during synthesis. This work may guide the synthesis of other SC-NMCs with even higher Ni content (Ni $\geqslant$ 80%), which feature more than 10% increase in energy density but face the same challenge in choosing synthesis temperature to achieve optimal particle size and structural ordering.

Acknowledgments

This work is supported by a junior faculty start-up grant of Shanghai Jiao Tong University (to L.S.L.), the Natural Science Foundation of China (22008154 to L.S.L., 21938005 to Z.F.M., and partially by 21991150 and 21991153), and partially by Sinopec (420038-1 to L.S.L). Stanford Synchrotron Radiation Lightsource of the SLAC National Accelerator Laboratory is supported by the U.S. DOE, Office of Science, Office of Basic Energy Sciences under Contract No. DE-AC02-76SF00515.

ORCID

Guannan Qian https://orcid.org/0000-0002-7000-8767
Linsen Li https://orcid.org/0000-0002-1105-9070

References

1. W. Li, E. M. Erickson, and A. Manthiram, *Nat. Energy*, **5**, 26 (2020).
2. S.-T. Myung, F. Maglia, K.-J. Park, C. S. Yoon, P. Lamp, S.-J. Kim, and Y.-K. Sun, *ACS Energy Lett.*, **2**, 196 (2017).
3. A. Manthiram, J. C. Knight, S.-T. Myung, S.-M. Oh, and Y.-K. Sun, *Adv. Energy Mater.*, **6**, 1501010 (2016).
4. W. Lee, S. Muhammad, C. Sergey, H. Lee, J. Yoon, Y.-M. Kang, and W.-S. Yoon, *Angew. Chem. Int. Ed.*, **59**, 2578 (2020).
5. S. Zheng et al., *J. Power Sources*, **412**, 336 (2019).
6. L. Mu, Q. Yuan, C. Tian, C. Wei, K. Zhang, J. Liu, P. Pianetta, M. M. Doeff, Y. Liu, and F. Lin, *Nature Commun.*, **9**, 2810 (2018).
7. Y. Yang et al., *Adv. Energy Mater.*, **9**, 1900674 (2019).
8. Y. Mao et al., *Adv. Funct. Mater.*, **29**, 1900247 (2019).
9. G. W. Nam, N.-Y. Park, K.-J. Park, J. Yang, J. Liu, C. S. Yoon, and Y.-K. Sun, *ACS Energy Lett.*, **4**, 2995 (2019).
10. W. Liu, P. Oh, X. Liu, M.-J. Lee, W. Cho, S. Chae, Y. Kim, and J. Cho, *Angew. Chem. Int. Ed.*, **54**, 4440 (2015).
11. P. Hou, J. Yin, M. Ding, J. Huang, and X. Xu, *Small*, **13**, 1701802 (2017).
12. U.-H. Kim, S.-T. Myung, C. S. Yoon, and Y.-K. Sun, *ACS Energy Lett.*, **2**, 1848 (2017).
13. T. Weigel, F. Schipper, E. M. Erickson, F. A. Susai, B. Markovsky, and D. Aurbach, *ACS Energy Lett.*, **4**, 508 (2019).
14. C. S. Yoon, U.-H. Kim, G.-T. Park, S. J. Kim, K.-H. Kim, J. Kim, and Y.-K. Sun, *ACS Energy Lett.*, **3**, 1634 (2018).
15. D. Kong et al., *Adv. Energy Mater.*, **9**, 1901756 (2019).
16. G.-L. Xu et al., *Nat. Energy*, **4**, 484 (2019).
17. P. Yan, J. Zheng, J. Liu, B. Wang, X. Cheng, Y. Zhang, X. Sun, C. Wang, and J.-G. Zhang, *Nat. Energy*, **3**, 600 (2018).
18. Y. Cho, P. Oh, and J. Cho, *Nano Lett.*, **13**, 1145 (2013).
19. Y.-K. Sun, Z. Chen, H.-J. Noh, D.-J. Lee, H.-G. Jung, Y. Ren, S. Wang, C. S. Yoon, S.-T. Myung, and K. Amine, *Nature Mater.*, **11**, 942 (2012).
20. Y.-K. Sun, S.-T. Myung, B.-C. Park, J. Prakash, I. Belharouak, and K. Amine, *Nature Mater.*, **8**, 320 (2009).
21. K.-J. Park, H.-G. Jung, L.-Y. Kuo, P. Kaghazchi, C. S. Yoon, and Y.-K. Sun, *Adv. Energy Mater.*, **8**, 1801202 (2018).
22. H.-H. Ryu, K.-J. Park, D. R. Yoon, A. Aishova, C. S. Yoon, and Y.-K. Sun, *Adv. Energy Mater.*, **9**, 1902698 (2019).
23. Z. Xu et al., *Nature Commun.*, **11**, 83 (2020).
24. J. E. Harlow et al., *J. Electrochem. Soc.*, **166**, A3031 (2019).
25. H. Li, J. Li, X. Ma, and J. R. Dahn, *J. Electrochem. Soc.*, **165**, A1038 (2018).
26. G. Qian et al., *Energy Storage Mater.*, **27**, 140 (2020).
27. J. Li, A. R. Cameron, H. Li, S. Glazier, D. Xiong, M. Chatzidakis, J. Allen, G. A. Botton, and J. R. Dahn, *J. Electrochem. Soc.*, **164**, A1534 (2017).
28. H. Cha, J. Kim, H. Lee, N. Kim, J. Hwang, J. Sung, M. Yoon, K. Kim, and J. Cho, *Adv. Mater.*, **32**, 2003040 (2020).
29. Y. Kim, *ACS Appl. Mater. Interf.*, **4**, 2329 (2012).
30. J. Li, H. Li, W. Stone, R. Weber, S. Hy, and J. R. Dahn, *J. Electrochem. Soc.*, **164**, A3529 (2017).
31. H. Li, J. Li, N. Zaker, N. Zhang, G. A. Botton, and J. R. Dahn, *J. Electrochem. Soc.*, **166**, A1956 (2019).
32. H.-J. Noh, S. Youn, C. S. Yoon, and Y.-K. Sun, *J. Power Sources*, **233**, 121 (2013).
33. J. Zhao et al., *Adv. Energy Mater.*, **7**, 1601266 (2017).
34. W. Tang, H. Kanoh, and K. Ooi, *Electrochem. Solid-State Lett.*, **1**, 145 (1998).
35. J. H. Kim, S. T. Myung, and Y. K. Sun, *Electrochim. Acta*, **49**, 219 (2004).
36. M. Thirumal, P. Jain, and A. K. Ganguli, *Mater. Chem. Phys.*, **70**, 7 (2001).
37. A. Dash, R. Vaßen, O. Guillon, and J. Gonzalez-Julian, *Nature Mater.*, **18**, 465 (2019).
38. J. Zhou et al., *Nature*, **556**, 355 (2018).
39. T. Kimijima, N. Zettsu, and K. Teshima, *Crystal Growth & Design*, **16**, 2618 (2016).
40. T. Kimijima, N. Zettsu, K. Yubuta, K. Hirata, K. Kami, and K. Teshima, *J. Mater. Chem. A*, **4**, 7289 (2016).
41. J. Zhu and G. Chen, *J. Mater. Chem. A*, **7**, 5463 (2019).
42. B. Toby, *J. Appl. Crystal.*, **34**, 210 (2001).
43. D. Kramer and G. Ceder, *Chem. Mater.*, **21**, 3799 (2009).
44. J. C. Garcia, J. Bareño, J. Yan, G. Chen, A. Hauser, J. R. Croy, and H. Iddir, *J. Phys. Chem. C*, **121**, 8290 (2017).
45. W. Bao et al., *Nano Lett.*, **20**, 8832 (2020).
46. F. Wang, M. Ge, S. Wi, X. Liu, J. Bai, S. Ehrlich, D. Lu, W.-K. Lee, and Z. Chen, *Angew. Chem. Int. Ed.* (2020), In Press.